Assiut University Journal of Multidisciplinary Scientific Research (AUNJMSR)
Faculty of Science, Assiut University, Assiut, Egypt.
Printed ISSN 2812-5029
Online ISSN 2812-5037
Vol. 53(3): 366- 384 (2024)
https://aunj.journals.ekb.eg

Effect of cadmium content on the stabilization of tetragonal phase of zirconium dioxide nanostructure prepared by Sol-Gel method

Abdulaziz Abu El-Fadl[1,2], A. A. Abu-Sehly[1,2] and Rania A. El-Touny [*2]

[1] Faculty of Science, Physics Department, Assiut University, 71516 Assiut, Egypt
[2] Faculty of Science, Physics Department, Lab. of Smart Materials for Energy Futures, Assiut University, 71516 Assiut, Egypt

[*]Corresponding Author: Rania A. El-Touny; e-mail: a_rania49@yahoo.com

ARTICLE INFO
Article History:
Received: 2024-05-13
Accepted: 2024-06-23
Online: 2024-08-29

Keywords:
Nanostructured ZrO_2,
Tetragonal phase stabilization,
Sol-gel technique,
Cadmium doping.

ABSTRACT

Zirconia (ZrO_2) nanostructures doped with Cd ratios were synthesized using a sol-gel approach and analysed using various techniques, including X-ray diffraction (XRD), differential scanning calorimetry (DSC), Fourier transform infrared spectroscopy (FT-IR), scanning electron microscopy (SEM), ultraviolet-visible spectroscopy (UV-Vis), and energy dispersive X-ray (EDX) analyses. XRD patterns for pure ZrO_2 samples annealed at 400 °C-500 °C had a tetragonal phase, while for ZrO_2 doped with different cadmium ratios, the tetragonal phase appears at 200 °C or above, up to 700 °C. The DSC measurements revealed that, the monoclinic phase was visible at 800 °C for the pure zirconia sample, while it was seen above 800 °C for the Cd-doped zirconia samples indicating a stabilization of the tetragonal phase. The FT-IR spectra confirmed the presence of cadmium ions in the zirconia host lattice and the formation of nano-zirconia in the tetragonal phase. EDX analysis verified the absence of any other elements except Zr, Cd, and O. The optical analysis demonstrated a reduction in the band gap for Cd-doped zirconia compared to pure zirconia. SEM images showed that agglomeration and neck formation occurred with increasing Cd ratios in the zirconia lattice.

1. INTRODUCTION

Nanomaterials are gaining popularity due to their novel features and applications. Zirconia, or zirconium dioxide (ZrO_2) by its chemical name, is one of the unique transition metal oxides because of its characteristics: high coefficient of thermal expansion, high oxygen ion conduction, high refractive index, good thermal stability, high dielectric constant, high melting point, high chemical resistance [1], and high mechanical properties due to the martensitic tetragonal to monoclinic transition [2]. Zirconia has been used in various fields, such as thermal barrier coatings [1],

batteries [3], catalysts [4], oxygen sensors [5], biomedical applications [6], body implants (dental ceramics) [7-9], and also as multifunctional applications [10].

The crystal structure of ZrO_2 significantly affects its physical properties as well as the performance of ZrO_2-based devices [11]. Pure zirconia undergoes three polymorphic phases at different annealing temperatures: tetragonal, monoclinic, and cubic phases [11-13]. It has been discovered for bulk ZrO_2 that the monoclinic phase 'which, although thermodynamically stable, lacks any useful applications since, upon cooling from the high-temperature tetragonal phase, it forms a crack in the sintered zirconia material due to volume expansion (5 vol.%) and shear strain' can transform completely to the tetragonal phase in a reversible manner at temperatures above 1170 °C in normal conditions and the tetragonal phase to the totally cubic phase at a temperature greater than 2370 °C [2].

However, at the nanoscale, the same martensitic tetragonal-to-monoclinic transformation is extremely important for mechanical applications since it serves as the foundation for the transition toughening of ceramic components. Tuning the synthesis process as well as the conditions or doping the zirconia lattice with various cations can both result in the stabilization of t-ZrO_2 nanoparticles [1], and hence one can avoid these mechanical issues. Transformation from tetragonal to cubic phase can be achieved at room temperature by adding some stabilizers such as CaO, MgO, and Y_2O_3 [12].

Garvie [14], first proposed the theory that the spontaneous appearance of the tetragonal phase structure at a critical crystallite size at room temperature might be explained by the tetragonal form's lower surface free energy than the monoclinic form, while larger particle sizes would undergo a tetragonal to monoclinic phase transition. Murase et al. [15, 16], reported that water enhanced the crystal growth rate and catalysed the tetragonal phase to monoclinic phase transformation. However, domain barriers might also prevent the transition from tetragonal phase to monoclinic phase [17]. Osendi et al. [18], proposed that anionic vacancies with trapped electrons facilitated the early nucleation of tetragonal zirconia. Moreover, they postulated that defect centres influenced the metastability of the tetragonal phase. Therefore, the mechanism of the stability of the tetragonal phase at low temperatures is still under debate.

The preparation process and conditions have a significant effect on the phase structure of the synthesized zirconia. Phase development and transition strongly influence most of the properties of ZrO_2. Various methods have been used to produce nano-sized zirconia, such as precipitation, hydrothermal, spray pyrolysis, the sol-gel route, high-pressure spark plasma sintering, and physical vapor deposition (PVD) techniques. The chosen method should have some advantages, such as ease of use, low equipment costs, high-purity raw materials, a high degree of nanostructure homogeneity, a relatively low process temperature, and the absence of toxic waste. The sol-gel approach met these criteria and offered a range of basic materials to choose from. The sol-gel process produces materials by gelation from chemical solutions; it is a more precise way of

creating nanocrystalline materials. Such a chemical technique allows the control of grain size and phase formation at much lower temperatures, which is desirable.

Cadmium's role as a stabilizer has received less attention compared to other dopants. In this study, we present a simple and low-cost modified sol-gel method for producing ZrO_2 nanoparticles and investigate the effect of Cd-doped zirconium oxide prepared by the sol-gel process on the thermal stability of the material in air. Furthermore, we explore the improvement in their optical properties. Also, we demonstrate that Cd^{+2} ions can stabilize the tetragonal phase when applied by an impregnation method.

2. EXPERIMENTAL TECHNIQUE

2.1 materials

Zirconium oxychloride octahydrate, 98% extra pure ($ZrOCl_2.8H_2O$), cadmium chloride AR monohydrate ($CdCl_2.H_2O$), sodium hydroxide scales (NaOH), and ethyl alcohol (CH_3CH_2OH). All the chemicals were bought from the LABO CHEMIE PVT.LTD. company and used without further purification.

2.2 synthesis of pure zirconia and Cd-doped zirconia

Pure ZrO_2 and Cd-doped ZrO_2 ($Cd_x@ZrO_2$) were synthesized by the same preparation steps as the sol-gel technique. To prepare Cd-doped zirconia, $ZrOCl_2.8H_2O$ and $CdCl_2.H_2O$ with various cadmium concentrations (x=5%, 10%, 15%, 20%, 25%, and 30%) were dissolved in double-distilled water at 50 °C and stirred vigorously for 20 minutes until a clear solution was obtained. Then, NaOH was added dropwise to the solution while stirring continuously for 20 minutes without heating until a white gel formed. This gel was allowed to cool down to room temperature. To remove any residuals from the reaction, the solution was washed several times in an ultrasonic cleaner with double-distilled water and CH_3CH_2OH. After that, the gel was dried for 24 hours at 60 °C, and then the dried gel was crushed to a fine powder. This powder was used to study the onset of crystallization at different annealing temperatures ranging from 200 °C to 800 °C and to monitor the phase change for pure zirconia, and investigate the effect of doping with different cadmium ratios at different temperatures on the stabilization of the tetragonal phase of zirconia.

We can explain the use of an alkaline medium (NaOH) in the reaction process to achieve the proposed goal (stabilize the tetragonal phase) [19], and avoid the unusual transformation of zirconia when using an acid medium, where zirconia appears in a mixed phase at the beginning of crystallization with a high percentage of monoclinic phase, implying that the weaker bond energies of the hydroxyls present in the hydrous zirconia precipitated under acidic conditions [20]. And this contributes to our aim.

2.3 characterization

XRD patterns for pure zirconia powder and Cd-doped zirconia nanoparticles were obtained at ambient temperature using a Philips PW 1710 diffractometer with CuK_{α} radiation and a graphite monochromator (λ=1.54056 Å) operating at an applied voltage of 40 KV and a current of 30 mA. The measuring angles ranged from 4° to 80°, and the scan rate was 0.06° per minute. DSC analysis was performed using a STA PT/1600 simultaneous DSC-TGA instrument with a standard error of ±1˚. Powder samples were placed in a crucible cell and heated at a rate of 10 °C per minute up to 1000 °C. The transmittance (T) for the prepared samples was determined using the NICOLET FTIR 6700 spectrometer by applying the KBr pellets method in the wavenumber range of 4000-500 cm^{-1}. The absorbance (A) spectra were measured at normal incidence at room temperature in the wavelength range of 200-900 nm using a computerized UV-visible spectrophotometer model JASCO V-770 with a 1 nm step. Elemental analysis was performed using EDX data, which were evaluated using a scanning electron microscope model, ULTRADRY QUANTA FEG 250 (Field Emission Gun), connected to an EDX unit. The JSM-T200 Jeol-Japan SEM apparatus was used to analyse the surface morphology of the powder samples.

3. RESULTS AND DISCUSSION

3.1 XRD analysis

The XRD spectra for pure ZrO_2 and ZrO_2 doped with different Cd ratios and annealed at different annealing temperatures are shown in Figures 1&2. The XRD patterns revealed the crystallinity, phases (crystal structure), and crystallite size of the produced nanopowder. All significant peaks in the XRD pattern were indexed using ICDD cards no. 79-1768 for the tetragonal phase and no. 37-1484 for the monoclinic phase. The calculated lattice parameters for pure zirconia and zirconia doped with different concentrations of cadmium ions ($Cd_x@ZrO_2$) (x=5%, 10%, 15%, 20%, 25%, and 30%) in the tetragonal and monoclinic phases are tabulated in Table 1.

The analysis of these patterns is divided into two parts: general characterization, which examines each incorporation ratio to evaluate the effects of thermal treatment at different annealing temperatures, and detailed characterization. The latter part focuses on Cd inclusion, tetragonal phase stability, and the role of heating and substitution in stabilizing the tetragonal phase up to higher annealing temperatures in order to track the crystallization of the tetragonal phase. The monoclinic phase is a new crystallizing phase that emerges by annealing dried powders at high temperatures. Since the main goal of this investigation is to stabilize the tetragonal phase, the maximum annealing temperature for each inclusion ratio is determined by the point at which all the peaks of the tetragonal phase completely disappear. Figure 1(a) indicates that the XRD patterns for pure zirconia samples annealed at temperatures below 400 °C is amorphous like the as-prepared samples, and those annealed between 400 °C and 500 °C is crystalline, with the tetragonal phase as the beginning of the crystallization. Samples annealed at 600 °C and

700 °C showed mixed tetragonal and monoclinic phase patterns, while samples annealed at 800 °C underwent almost complete monoclinic phase transformation.

Table 1: Lattice parameters of the tetragonal and monoclinic phases for pure zirconia and Cd-doped zirconia nanoparticles obtained from XRD patterns.

Crystalline phase	Lattice parameters	Doping concentration						
		0%	5%	10%	15%	20%	25%	30%
Tetragonal phase	a = b (Å)	3.6000	3.5983	3.6023	3.6190	3.6042	3.6183	3.6113
	C (Å)	5.1674	5.1907	5.2063	5.1316	5.1969	5.1481	5.0925
	Volume ($Å^3$)	66.97	67.21	67.56	67.21	67.51	67.41	66.41
Monoclinic phase	a (Å)	5.3053	5.3162	5.3159	5.3130	5.3028	5.3180	5.3122
	b (Å)	5.2108	5.2050	5.2050	5.2198	5.2112	5.2066	5.2116
	c (Å)	5.1355	5.1473	5.1471	5.1460	5.1329	5.1451	5.1435
	β^* (°)	99.26	99.14	99.14	99.12	99.32	99.26	99.26
	Volume ($Å^3$)	140.12	140.6	140.6	140.9	140.1	140.6	140.5

Incorporation of Cd ions stabilizes the tetragonal phase at much lower temperatures than for pure zirconia (200 °C and 300 °C), and also for a wider range of temperatures. ZrO_2 doped with small ratios of Cd ions (5% and 10%) that annealed at 200 °C showed all peaks for the tetragonal phase, but with a shift in the peak position. Increasing the incorporation of the Cd ratio (15%, 20%, and 25%) at the same temperature results in only the main peak for the tetragonal phase (101). However, 30% Cd-doped zirconia ratio samples show an amorphous phase (Figure 1(b)). For 5%, 10%, 15%, and 20% Cd-doped ZrO_2 annealed at 300 °C, the obtained structure was tetragonal, and the same structure was also obtained for samples doped with a 25% cadmium ratio but with low intensity peaks. Samples doped with a 30% Cd ratio showed an amorphous structure at this temperature (Figure 1(c)). This can be explained by the fact that increasing the dopant ratio requires more energy to achieve a complete and stable tetragonal phase.

The samples of ZrO_2 doped with Cd ratios of 5%, 10%, 15%, 20%, and 25%, which annealed at 400 °C, were maintained in the tetragonal phase, and for ZrO_2 doped with 30% Cd, the samples still looked amorphous, (Figure 1(d)), but the tetragonal phase became clearly visible at 500 °C to 600 °C for all Cd doped ratios (Figure 1(e), and 2(a)). However, when the temperature increased to 700 °C, the samples doped with Cd ratios of 5%, 10%, and 15% showed a metastable state between the tetragonal and monoclinic phases, which we call in simple words a mixed phase, but it can be noticed that the ratio of the tetragonal phase gradually increased with increasing Cd ratio from 5% to 15%, (Figure 2(b)). Samples annealed at 800 °C doped with the proposed Cd ratios displayed a typical monoclinic phase, revealing peaks positioned at 24.0°, 28.0°, 31.1°, 32.8°, 34.1°, 35.0°, 45.0°, 49.1°, 50.0°, 54.0°, 55.3°, 59.7°, 65.6°, and 71.1° corresponding to (110), (-111), (111), (200), (020), (-112), (211), (220), (022), (003), (122), (131), (023) and (-223) planes, respectively, which are in high agreement with card no. ICDD 37-1484 as shown in (Figure 2(c)). A more precise way to say it is that the samples with ratios of

20%, 25%, or 30% skipped any metastable phases at any of the annealing temperatures and went directly from the tetragonal phase to the monoclinic phase.

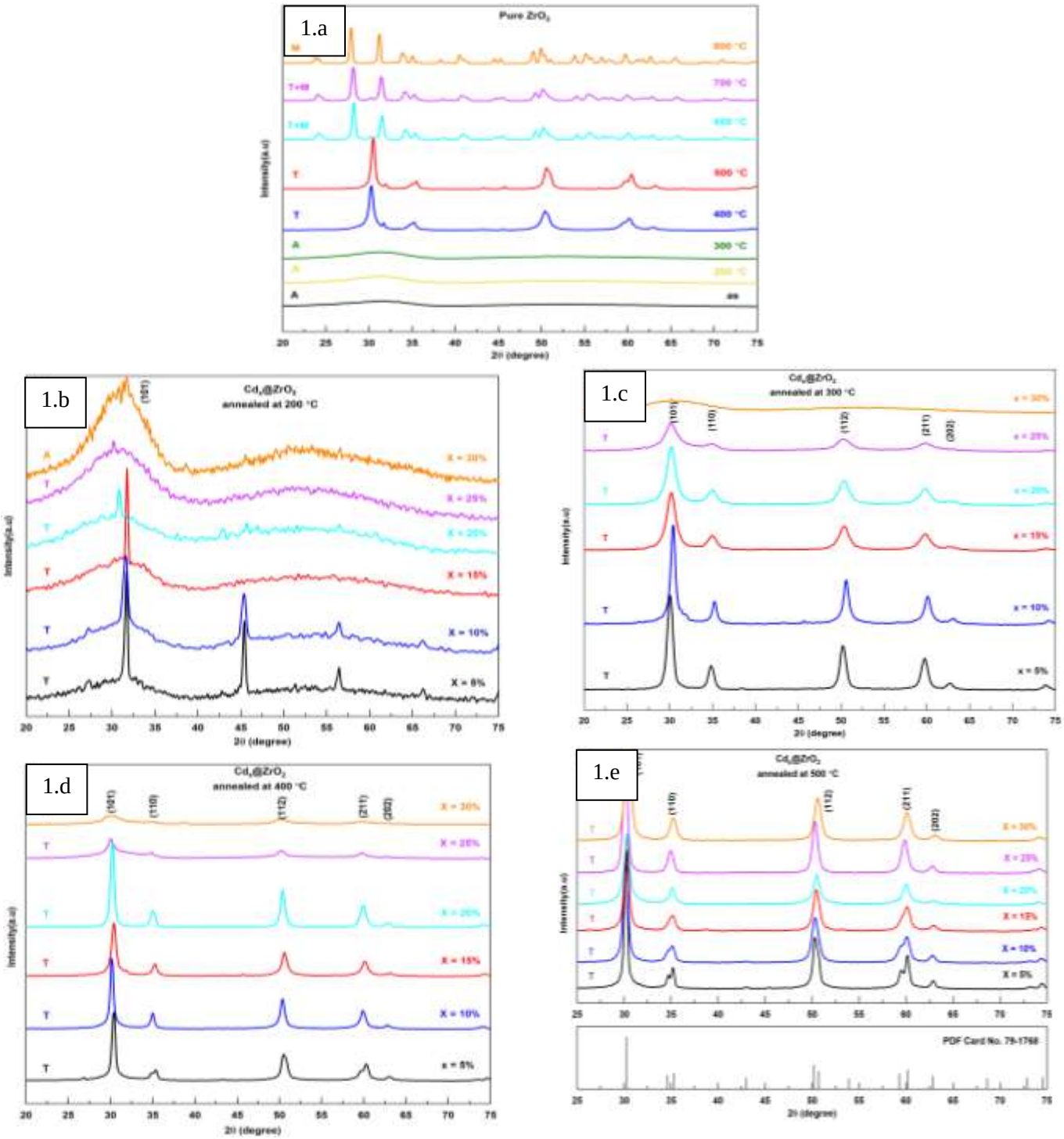

Figure 1 (a): XRD patterns for pure ZrO_2 samples annealed at 200 °C to 800 °C; (b, c, d, and e): XRD patterns for ZrO_2 nanostructured doped with different Cd ratios (x= 5%, 10%, 15%, 20%, 25%, and 30%), annealed at 200 °C, 300 °C, 400 °C, and 500°C, respectively.

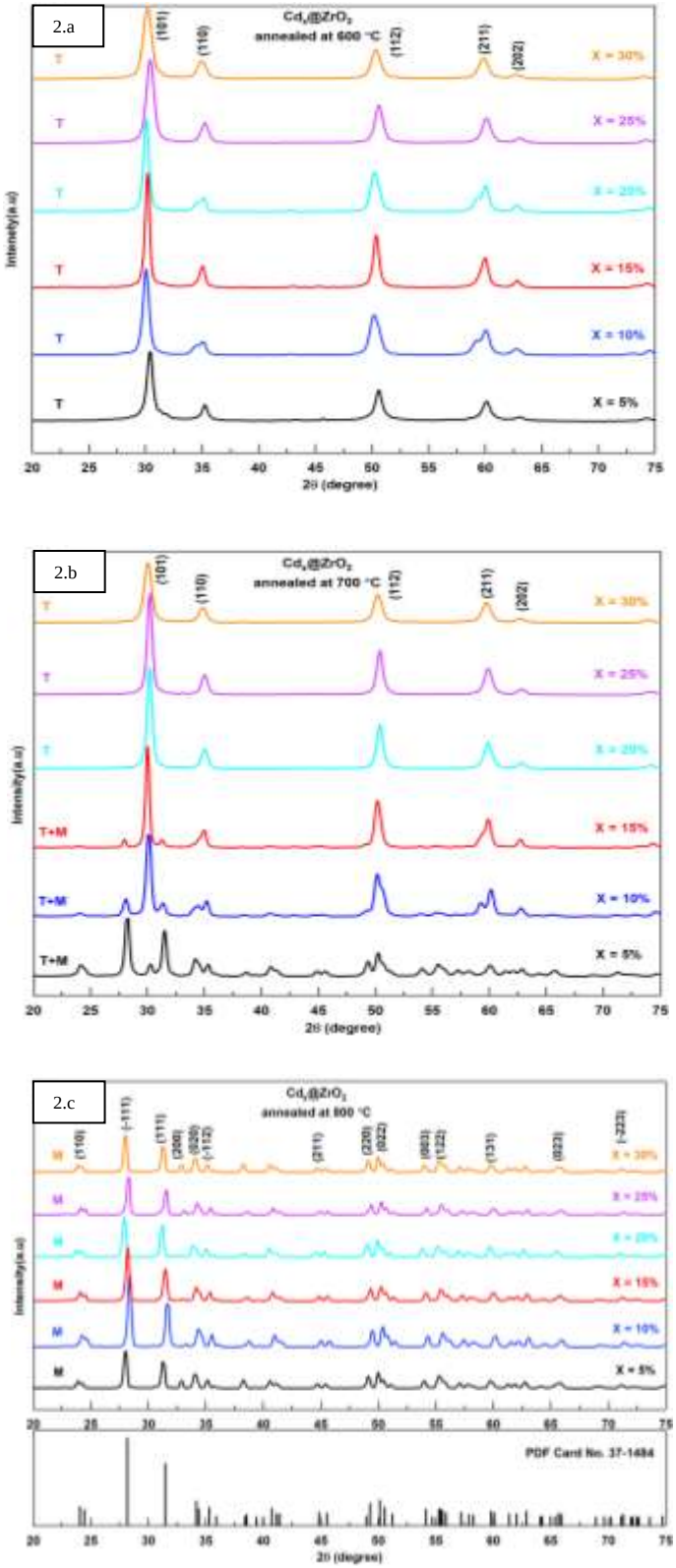

Figure 2 (a, b, and c): XRD patterns for ZrO_2 nanostructured doped with different Cd ratios (5%, 10%, 15%, 20%, 25%, and 30), annealed at 600 °C, 700 °C, and 800 °C, respectively.

As can be seen from Figures 1 and 2, the XRD patterns for samples doped with different Cd ratios and annealed at different annealing temperatures developed two main crystalline phases (the tetragonal phase and the monoclinic phase). The tetragonal phase peak profile (101, 110, 112, 211, and 202 at positions of 2θ = 30.18°, 35.0°, 50.4°, 60.0°, and 63.1°, respectively) matches ICDD card no. 79-1768, indicating that there are no impurities or Cd-related peaks (Cd has been successfully incorporated in the zirconia lattice). This could be explained by the slight difference in ionic radius between host Zr^{+4} (0.16 nm) and Cd^{+2} dopant (0.154 nm). As a result, Cd ions replaced Zr ions in the host lattice with ease. All the diffraction patterns had large peaks, indicating that the materials were nanocrystalline as prepared.

Table 1 show that the lattice parameters of ZrO_2 nanoparticles doped with different Cd ions are not significantly different from the lattice parameters of pure zirconia nanoparticles, which confirming that cadmium has been successfully incorporated into the zirconia lattice.

The volume fraction of the tetragonal phase (V_t) was calculated by first computing the average peak areas of the corresponding tetragonal $(101)_t$ plane and monoclinic planes $(-111)_m$, $(111)_m$ and then applying the following formula [21], and the obtained data are listed in Table 2.

$$Vt\frac{A(101)t}{A(111)m + A(-111)m + A(101)t} \quad (1)$$

From the phase ratio of pure zirconia to that of the zirconia with the highest ratio of Cd doping (30% Cd), we can clearly see how adding Cd ions and increasing their proportion affects the stabilization of the tetragonal phase, as shown in Figure 3. From our study of samples annealed at different temperatures (from 200 °C to 800 °C with a 100 °C step), we find that for pure zirconia, the tetragonal phase starts at 400 °C and becomes a mixed phase with a dominant monoclinic phase ratio (97.8% as calculated in Table 2) at 600 °C. Therefore, we further investigated the phase change between 500 °C and 600 °C with a 20 °C step. The study revealed that the tetragonal phase ratios were 92.48%, 34.88%, 26.2%, 9.6%, and 3% at temperatures of 510 °C, 530 °C, 550 °C, 570 °C, and 590 °C, respectively.

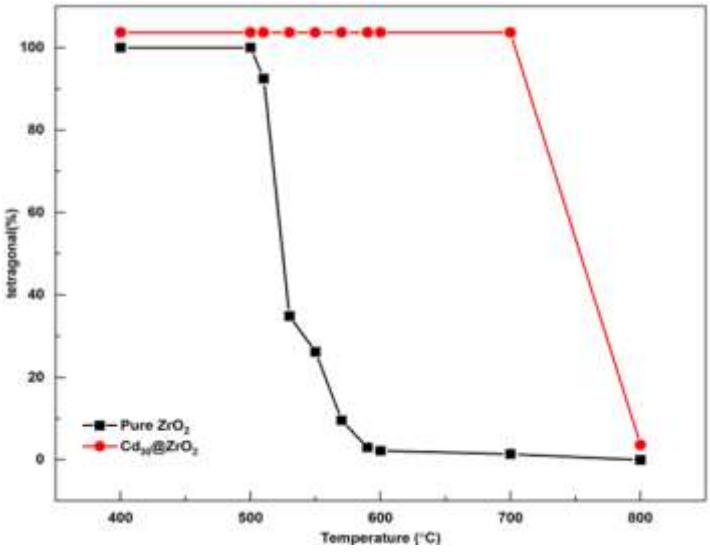

Figure 3: The influence of cadmium doping on the samples that annealed at 200 °C up to 800 °C.

The average crystallite size (D) for tetragonal zirconia was calculated based on the full width at half maximum intensity parallel to the (101) plane for the tetragonal phase and the (-111, 111) reflection for the monoclinic phase, with peak deconvolution for mixed phase samples, using Scherrer's equation [22].

$$D = \frac{k\lambda}{\beta_{FWHM}\cos\theta} \quad (2)$$

Where λ is the wavelength of CuK_α radiation, k is a minor factor with a value of 0.94, β_{FWHM} is the full width at half maximum measured in radians, and θ is Bragg's diffraction angle.

The theoretical density (ρ) can be estimated from the X-ray diffraction pattern using the formula [23].

$$\rho = \frac{ZM}{N_A V} \quad (3)$$

Where Z is the number of molecules per unit cell (Z = 4 for the monoclinic phase and 2 for the tetragonal phase), V is the unit cell volume, N_A is Avogadro's number, and M is the molecular weight of the composition.

The strain (ε) in the packed structure can also be calculated using the Williamson-Hall (W-H) formula [24].

$$\varepsilon = \frac{\beta_{FWHM}}{4\tan\theta} \quad (4)$$

The peak position is adjusted according to the strain value. This causes a change in the lattice constants and the estimated strain values.

The crystallite size is used, and the dislocation density (δ) is calculated using equation [25].

$$\delta = \frac{1}{D^2} \quad (5)$$

The average grain size D (nm), dislocation density δ $(nm)^{-2}$, density ρ (g/cm^3), and strain ε for pure and Cd-doped zirconia nanoparticles in the tetragonal and monoclinic phases are listed in Table 3.

Table ٣ shows that the average crystallite size calculated for the pure tetragonal zirconia nanoparticles is about 10.2 nm. This is consistent with the expected range reported by Garvie [14], (D less than 10 nm). The table also clearly shows that the crystallite size for pure zirconia increases automatically from 10.2 to 17.9 nm when the calcination temperature increases from 400 to 800 °C.

Moreover, we can observe that the crystallite size decreases from 14.3 nm for the 5% Cd ratio to 9.4 nm in the highest ratio of 30% Cd for the same annealing temperature as a result of maintaining the tetragonal phase at higher temperatures. Furthermore, since Cd and Zr ions have different atomic radii, with Cd ions being smaller than Zr ions,

increasing the ratio of Cd ions reduces the host lattice size. which explains how Cd ions stabilize the tetragonal phase of zirconia.

For pure zirconia, the dislocation density and strain decrease systematically when the tetragonal phase transforms to the monoclinic phase as a result of increasing crystallite size with increasing temperatures. For the same ratio of Cd-doped zirconia, dislocation density and strain also decrease when changing from the tetragonal phase to the monoclinic phase for the same reason as in pure zirconia, but when comparing different ratios of Cd-doped zirconia for the same phase, we find that both δ and ε increase with increasing the ratio of doping as a result of stabilizing the tetragonal phase.

Table 2: Volume fraction of tetragonal phase (V_t%) percentage for pure zirconia and Cd-doped zirconia nanoparticles at various annealing temperatures.

	Doping concentration	Annealing Temperatures (°C)						
		200 °C	300 °C	400 °C	500 °C	600 °C	700 °C	800 °C
Phase ratio (%)	0%	-	-	T	T	T=2.2% M=97.8%	T=1.4% M=98.6%	M
	5%	T	T	T	T	T	T=6.4% M=93.6%	M
	10%	T	T	T	T	T	T=72.2% M=27.8%	M
	15%	T	T	T	T	T	T=92.0% M=8.0%	M
	20%	T	T	T	T	T	T	M
	25%	T	T	T	T	T	T	M
	30%	A	A	A	T	T	T	M

Table 3: The average grain size D (nm), dislocation density δ $(nm)^{-2}$, density ρ (g/cm^3), and strain ε for pure and Cd-doped zirconia nanoparticles in the tetragonal and monoclinic phases.

Crystalline phase	Structure parameter	Doping concentration						
		0%	5%	10%	15%	20%	25%	30%
Tetragonal phase	D (nm)	10.2	14.3	13.0	12.0	11.0	10.0	9.4
	δ $(nm)^{-2}$	0.009	0.004	0.006	0.005	0.009	0.008	0.011
	ρ (g/cm^3)	6.90	6.93	6.94	7.03	7.05	7.12	7.28
	Strain ε	0.003	0.002	0.002	0.002	0.003	0.003	0.003
Monoclinic phase	D (nm)	17.9	23.9	23.8	21.0	21.6	22.7	24.2
	δ $(nm)^{-2}$	0.003	0.0017	0.0022	0.0017	0.0021	0.0019	0.0017
	ρ (g/cm^3)	6.59	6.62	6.67	6.71	6.80	6.82	6.88
	Strain ε	0.001	0.0014	0.0016	0.0014	0.0015	0.0014	0.0013

3.2 DSC analysis

Thermal analysis shows the suitable temperature for the calcination process to obtain the desired structure and confirms the structure obtained from XRD analysis. Figure 4 shows the DSC scan for as-prepared pure zirconia and Cd-doped zirconia with selected Cd concentrations (from x = 15% to x = 30%). It clearly shows that the peak for the tetragonal phase is centred at around 450 °C for pure zirconia and around 500 °C for the selected Cd ratios, with a small shift as indicated in the XRD data. This shift confirms that with an increase in Cd percentage, the tetragonal phase forms at higher temperatures. While the peak for the monoclinic phase is cantered around 800 °C for pure zirconia and shifted towards a higher temperature for Cd-doped ZrO_2 ratios as a result of stabilizing the tetragonal phase, these results are the proposed aim of this study. Furthermore, these results agree well with those obtained from XRD measurements.

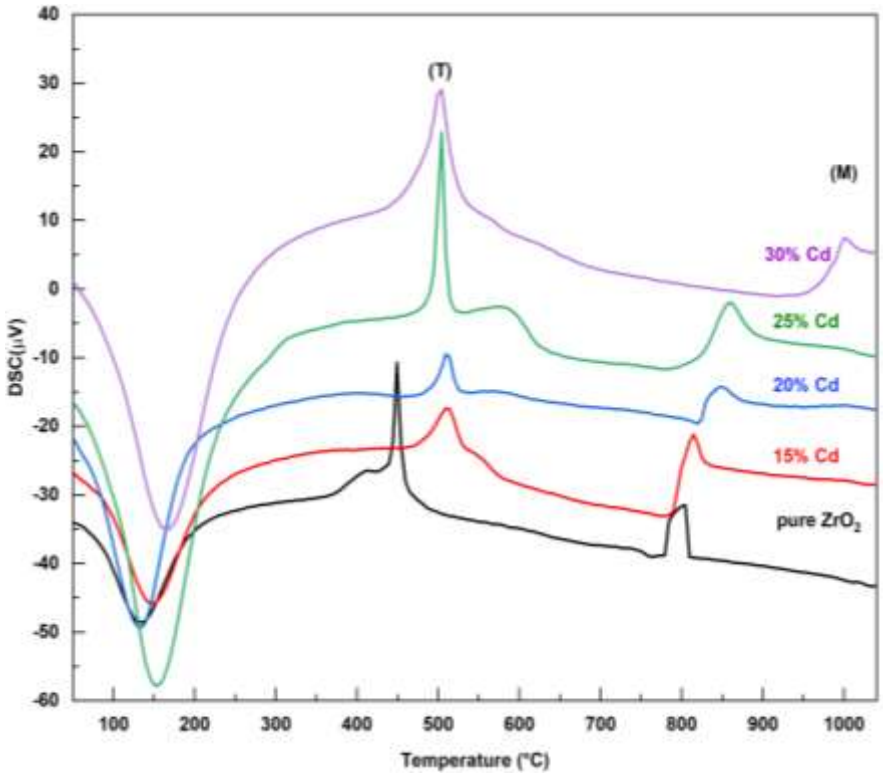

Figure 4: DSC for the as-prepared pure zirconia and Cd-doped zirconia with selected cadmium concentrations.

3.3 phase composition analysis (FT-IR)

FT-IR spectroscopy was used to investigate the vibrational bonds of the pure and Cd-doped zirconia in the tetragonal phase, as shown in Figure 5, in addition to detect any changes that occur due to doping. The powder was calcined to the tetragonal phase at 500 °C for pure zirconia and at 600 °C for Cd-doped zirconia ratios. Pure zirconia samples show only three peaks: a broad band exists around 3500 cm^{-1}, which corresponds to the stretching vibrations of O-H; the other broad band is around 1600 cm^{-1}, which is

related to the bending vibrations of O-H due to the presence of water on the gel particles [26], and the peak at 493 cm^{-1}, which corresponds to the tetragonal stretching of Zr-O [26, 27]. The obtained data are fully consistent with those presented in [28, 29].

FTIR spectra for $Cd_x@ZrO_2$ (from x = 5% to x = 30%) reveal the same peaks as pure ZrO_2, with a small shift to a higher wavenumber region due to the change in the bond lengths, which can be attributed to the introduction of Cd ions, in addition to three other peaks. The peak around 3500 cm^{-1} represents O-H stretching but is stronger than that for the pure one, which suggests that adding Cd ions to the zirconia lattice increases surface hydroxylation, and these hydroxyls are responsible for the tetragonal phase [19]. The peak around 1620 cm^{-1} represents O-H bending, and the peak exists between 470 cm^{-1} and 500 cm^{-1} for tetragonal Zr-O stretching as well. Besides the peaks appearing for pure zirconia samples, there is a minor peak around 620 cm^{-1} related to tetragonal Zr-O bending [30], and a less intense peak between 900 cm^{-1} and 990 cm^{-1} for the t-zirconia Zr = O stretching mode [28], which starts to appear in the 10% Cd-doped ZrO_2 as a result of strengthening the tetragonal phase with doping. These peaks disappeared in the pure zirconia and became clear in the Cd-doped zirconia. Therefore, FT-IR spectroscopy confirms the formation of the tetragonal phase in pure zirconia and its enhancement in Cd-doped zirconia nanoparticles, and these are significant results for the proposed aim (stabilization of the tetragonal phase), which is consistent with XRD and DSC analyses. Another additional peak is the characteristic peak for Cd-O stretching around 1100 cm^{-1} [31], which is the main difference from the pure zirconia FT-IR. The assignments of FT-IR bands are presented in Table 4.

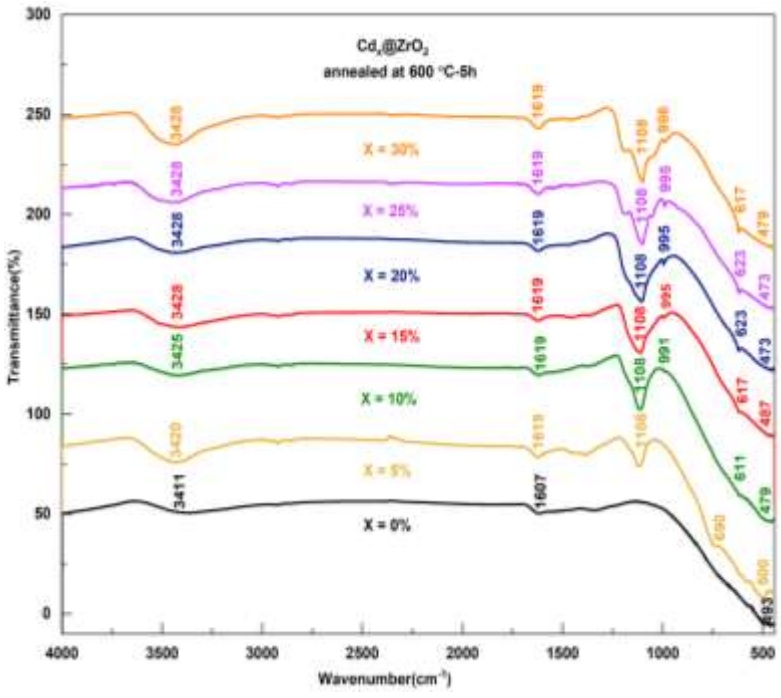

Figure 5: FT-IR spectra for pure zirconia and Cd-doped zirconia nanoparticles in the tetragonal phase.

Table 4: FT-IR vibrational bonds for pure zirconia and Cd-doped zirconia nanoparticles in the tetragonal phase.

Sample name	Wavenumber (cm^{-1})	Bond
Pure ZrO_2	around 3500 cm^{-1}	O-H stretching
	around 1600 cm^{-1}	O-H bending
	around 500 cm^{-1}	t-Zr-O stretching
Cd-doped ZrO_2	around 3500 cm^{-1}	O-H stretching
	around 1620 cm^{-1}	O-H bending
	between 470-500 cm^{-1}	t-Zr-O stretching
	around 620 cm^{-1}	t-Zr-O bending
	between 900-990 cm^{-1}	t-Zr = O stretching
	around 1100 cm^{-1}	Cd-O stretching

3.4 Elemental analysis (EDX)

To identify the elemental composition of the prepared samples and verify their purity, EDX analysis, which is a qualitative method, was employed. The EDX analysis for pure zirconia samples annealed at 500 °C (tetragonal phase), shown in Figure 6, reveals only Zr and O peaks, with no significant impurities. While the Cd-doped zirconia samples annealed at 600 °C (tetragonal phase), have Zr, O and Cd peaks. It is clearly demonstrating that the intensity of Cd-related peaks increased as its percentage increased. Table 5 shows that by increasing the Cd doping ratio, the Zr percentage decreased, implying that Cd ions substituted Zr ions in the host lattice, resulting in a suppression of the tetragonal to monoclinic transformation (stabilization). Therefore, we can conclude that the EDX data are consistent with the XRD, DSC and FT-IR data.

Table 5: Elemental composition for selected samples of $Cd_xZr_{1-x}O_2$ (x = 5%, 10%, 20% and 30%).

Element	Zr		O		Cd	
	Wt.%	At. %	Wt.%	At. %	Wt.%	At. %
ZrO_2	78.0	38.9	20.9	59.3	0	0
5% Cd- ZrO_2	73.6	35.5	23.0	63.1	3.5	1.4
10% Cd- ZrO_2	66.7	30.1	26.2	67.4	7.0	2.6
20%Cd- ZrO_2	51.0	23.7	25.4	67.4	23.5	8.9
30%Cd- ZrO_2	50.5	23.7	25.0	67.0	24.4	9.3

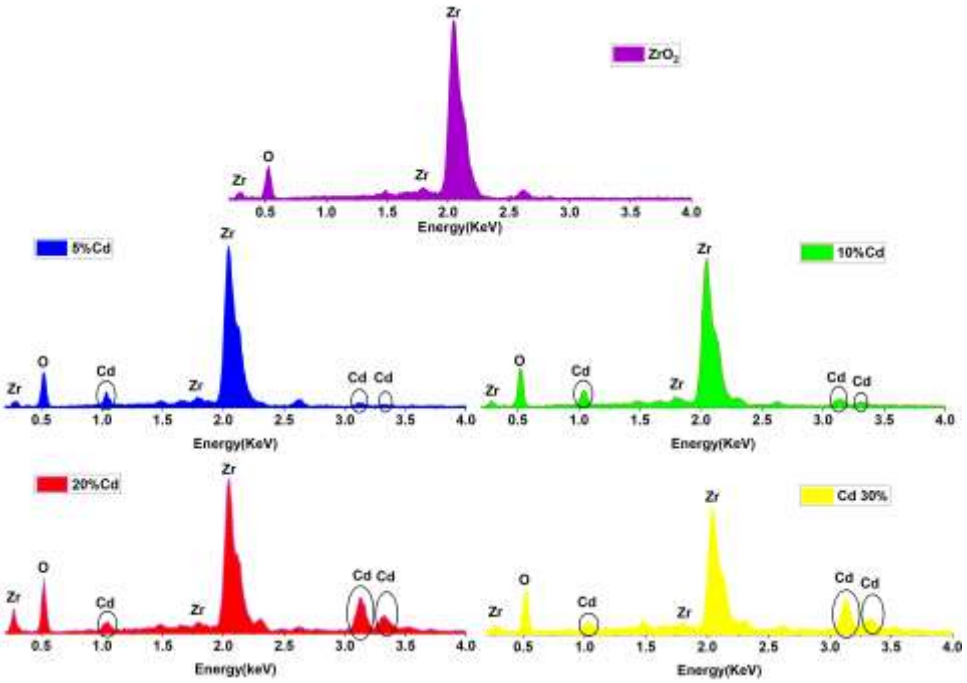

Figure 6: EDX spectra for pure zirconia and Cd-doped zirconia nanoparticles in the tetragonal phase.

3.5 optical analysis

UV-Vis absorbance spectra were used to study how the optical properties of ZrO_2 nanostructures changed when doped with different Cd ratios. The Beer-Lambert law employed to compute the absorption coefficient (α) in terms of the absorbance A [32].

$$\alpha = \frac{A}{cL} \tag{6}$$

Where c is the concentration of the suspension, L is the optical path length, and here is 1 cm.

Tauc's law [33], which describes the relationship between incident photon energy and the absorption coefficient of semiconductor materials, was used to calculate the band gap of the fabricated samples.

$$(\alpha h\nu)^2 = B(h\nu - E_g)^n \tag{7}$$

Where B is a probability constant, h is Planck's constant, and ν is the optical frequency, so that hν is the energy of the incident photon, E_g is the optical band gap energy, and n is an exponent whose value depends strongly on the type of the electronic transition. Therefore, n takes 1/2 for the direct transition and 2 for the indirect transition.

In this study, Figure 7(a), (b), and Table 6 show that the pure tetragonal zirconia prepared by the sol-gel technique has E_g = 4.30 eV and that Cd-doped zirconia has

E_g = 2.80 eV, 2.70 eV, 2.25 eV, 2.10 eV, 2.00 eV, and 1.80 eV for x ratios of 5%, 10%, 15%, 20%, 25%, and 30%, respectively. This reduction in the optical band gap may be due to the creation of high oxygen vacancies resulting from the introduction of cadmium ions in the zirconia lattice. According to Osendi et al. [18] 'anionic vacancies with trapped electrons promote the early nucleation of t-ZrO_2'. As a result, new energy levels emerge near the top of the valence band and the bottom of the conduction band. These are good results for Cd-doped zirconia compared to the results obtained by Ahmed W. et al. [28], who used the facile co-precipitation method for Fe-doped zirconia and obtained an optical band gap of 3.7 eV for pure zirconia, and 2.1 eV as the optimal value for 10% Fe-doped zirconia. They are also better than the results of Rajesh et al. [34], who used the facile precipitation method and obtained an optical band gap of 5.12 eV for pure zirconia and reduced it to 3.15 eV for 8% Ni-doped zirconia, and Rani et al. [35], who used the sol-gel route, and obtained 5.32 eV for pure zirconia, then reduced it to 5.06 eV for 7% Ag-doped zirconia nanoparticles.

Table 6 indicated that for zirconia doped with different Cd ratios and annealed at 600 °C (tetragonal phase), both the band gap and the crystallite size decreases, which contradicts the general assumption that the band gap decreases as the size increases. We can explain this contradiction in terms of the temperature as follows: The tetragonal phase starts at different temperatures for different ratios. For example, with 5% Cd-doped zirconia, the tetragonal phase starts at 200 °C (Figure 1(b)), and continues to 600 °C, at which it has the largest crystallite size for the tetragonal phase, then it begins to mix with 93.6% monoclinic at 700 °C. On the other hand, for 30% Cd-doped zirconia, the tetragonal phase starts at 500 °C (Figure 1(e)), and continues to 700 °C (Figure 2(b)), so it has the smallest crystallite size at 500 °C.

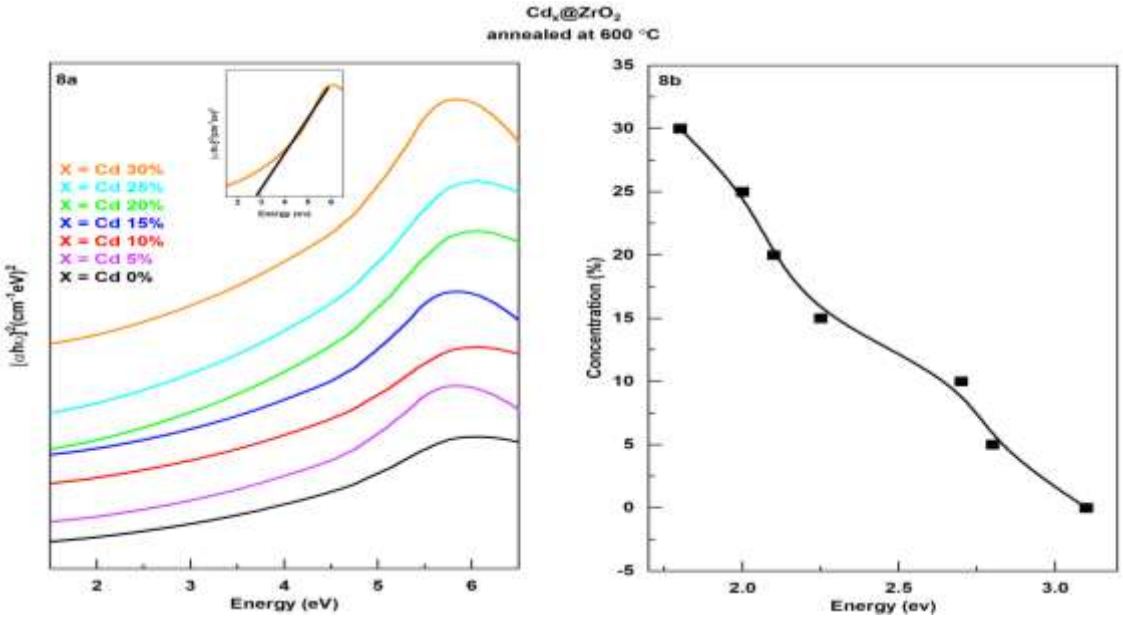

Figure 7 (a): Tauc'c plot, and (b) optical band gap for pure zirconia and Cd-doped zirconia with different cadmium concentrations in the tetragonal phase.

3.5 morphological analysis (SEM)

To qualitatively evaluate the microstructure of the synthesized samples, scanning electron microscopy (SEM) is carried out. Figure 8 shows the SEM images of pure and Cd-doped zirconia for the selected ratios of (x = 5%, 10%, 15%, and 30%) and annealed at 600 °C (tetragonal phase). It is evident from the figure that pure and Cd-doped zirconia have the same morphology and that the produced nanoparticles have an irregular sheet shape, a quasi-symmetrical morphology and a uniform size distribution. It can be clearly observed that these sheets were covered with small spherical agglomerates (more compact); the particles are connected to each other in a random manner, which is why agglomeration and neck formation occur with increasing the ratio of Cd doping.

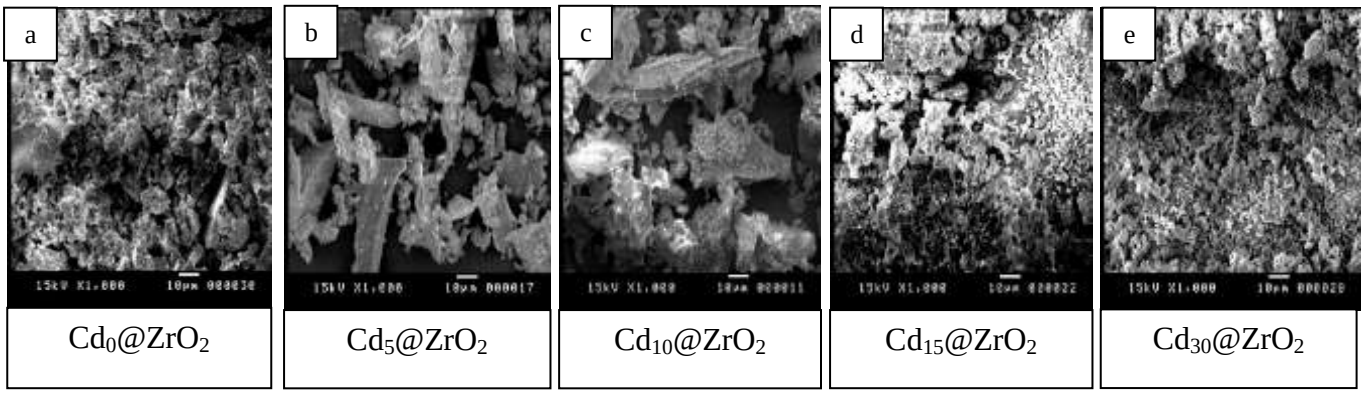

Figure 8 (a): SEM images for pure zirconia, (b) SEM images for 5% Cd-doped zirconia, (c) SEM images for 10% Cd-doped zirconia, (d) SEM images for 15% Cd-doped zirconia, (e) SEM images for 30% Cd-doped zirconia. All have the same magnifications (15 KV *1000).

4. CONCLUSION

Pure zirconia NPs and $Cd_x@ZrO_2$ ($0 \leq x \geq 30$) were successfully synthesized by using the sol-gel method. XRD patterns demonstrated that pure zirconia is amorphous below 400 °C and started its tetragonal phase crystallization from 400 °C to 500 °C, then transformed to a mixed phase (T+M) with a very small tetragonal ratio at 600 °C and went to a complete monoclinic phase at 800 °C. While for small ratios of Cd-doped zirconia (x = 5% and 10%) started with the tetragonal phase at an annealing temperature of 200 °C, the mixed phase started at a temperature of 700 °C, and finally a nearly complete monoclinic phase at 800 °C. Furthermore, for a large ratio of Cd-doped samples (x = 30%), the tetragonal phase appeared at 500 °C but remained till 700 °C and directly transitioned to the monoclinic phase at 800 °C. Therefore, adding Cd ions to the ZrO_2 lattice stabilizes the tetragonal phase, which is the most important phase for zirconia applications. This stabilization occurred at much lower temperatures, for a wider range of temperatures, and up to higher annealing temperatures than that for pure zirconia. Stabilization of the tetragonal phase was also confirmed using DSC and FT-IR analyses, in which DSC revealed that the peak related to the tetragonal phase was around 450 °C for pure zirconia and around 500 °C for all Cd ratios-doped zirconia, but the peak related

to the monoclinic phase appeared around 800 °C for pure zirconia and above for Cd-doped zirconia. FTIR spectroscopy revealed only hydroxyl group peaks and the peak related to stretching t-ZrO_2 for pure zirconia, but FTIR for Cd-doped zirconia shows the characteristic peak related to Cd-O and more peaks for t-Zr-O than those in pure zirconia. The detection of Zr, Cd, and O using energy dispersive X-ray spectroscopy (EDX) confirms the proposed formation of $Cd_xZr_{1-x}O_2$ nanoparticles. UV-visible spectroscopy shows a reduction in the optical band gap from 3.1 eV for pure zirconia to 1.8 eV for 30% Cd-doped zirconia. SEM images indicate that Cd-doped zirconia have the same morphology; they are irregular sheets with a quasi-symmetrical shape.

REFERENCES

[1] G. Balakrishnan, P. Kuppusami, D. Sastikumar, J. I. Song, Growth of nanolaminate structure of tetragonal zirconia by pulsed laser deposition, Nanoscale Res. Lett., 8 (2013) 1.
[2] S. Shukla, S. Seal, Mechanisms of room temperature metastable tetragonal phase stabilisation in zirconia, Int. Mater. Rev., 50 (2005) 45.
[3] L. Liu, Z. Wang, Y. Xie, Y. Peng, J. Dong, Y. T. Chow, G. Zhang, L. Zhu, X. Wang, D. Xu, Zirconia/polyethylene terephthalate ceramic fiber paper separator for high-safety lithium-ion battery, Ionics, 26 (2020) 6057.
[4] S. Chen, A. Tennakoon, K. E. You, A. L. Paterson, R. Yappert, S. Alayoglu, L. Fang, X. Wu, T. Y. Zhao, M. P. Lapak, M. Saravanan, R. A. Hackler, Y. Wang, L. Qi, M. Delferro, T. Li, B. Lee, B. Peters, R. K. Poeppelmeier, S. C. Ammal, C. R. Bowers, F. A. Perras, A. Heyden, A. D. Sadow, W. Huang, Ultrasmall amorphous zirconia nanoparticles catalyse polyolefin hydrogenolysis, Nat. Catal., 6 (2023) 161.
[5] Z. Luo, J. Xiao, F. Xia, Y. Yang, Preparation and characterization of zirconia oxygen sensors, J. Wuhan Univ. Technol.-Mater. Sci. Ed., 22 (2007) 612.
[6] A. V. Shevchenko, E. V. Dudnik, A. K. Ruban, V. P. Red'ko, L. M. Lopato, Nanocrystalline powders based on ZrO_2 for biomedical applications and power engineering, Powder Metall. Met. Ceram., 41 (2002) 558.
[7] A. A. Madfa, F. A. Al-Sanabani, N. H. Al-Qudami, J. S. Al-Sanabani, A. G. Amran, Use of zirconia in dentistry: An overview, open Biomater. J., 5 (2014) 1.
[8] Z. Özkurt, E. Kazazoğlu, Zirconia dental implants: A literature review, J. Oral Implantol., 37 (2011) 367.
[9] C. Hu, J. Sun, C. Long, L. Wu, C. Zhou, X. Zhang, Synthesis of nano zirconium oxide and its application in dentistry, Nanotechnol Rev., 8 (2019) 396.
[10] I. Danilenko, O. Gorban, A. Shylo, L. Akhkozov, M. Lakusta, T. Konstantinova, New multifunctional zirconia composite nanomaterials-from electronics to ceramics, Mater. Sci. Eng., 213 (2017) 1.
[11] M. Mokhtar, S. N. Basahel, T. T. Ali, Effect of synthesis methods for mesoporous zirconia on its structural and textural properties, J. Mater. Sci., 48 (2013) 2705.
[12] J. Cott Garcia, L. M. R. Scolfaro, A. T. Lino, V. N. Freire, G. A. Farias, C. C. Silva, H. W. Leite Alves, S. C. P. Rodrigues, E. F. da Silva Jr, Structural, electronic, and optical properties of ZrO_2 from ab initio calculations, J. Appl. Phys., 100 (2012) 1.
[13] M. M. Rashad, H. M. Baioumy, Effect of thermal treatment on the crystal structure and morphology of zirconia nanopowders produced by three different routes, J. Mater.

Process. Technol., 195 (2008) 178.
[14] R. C. Garvie, Stabilization of the tetragonal structure in zirconia microcrystals, J. Phys. Chem., 82 (1978) 218.
[15] Y. Murase, and E. Kato, Phase transformation of zirconia by ball-milling, Am. Ceram. Soc.-Discuss Notes, (1979) 527.
[16] Y. Murase, E. Kato, Role of water vapor in crystallite growth and tetragonal- monoclinic phase transformation of ZrO_2, J. Am. Ceram. Soc., 66 (1983) 196.
[17] T. I. M. T. Mitsuhashi, M. Ichihara, U. Tatsuke, Characterization and stabilization of metastable tetragonal ZrO_2, J. Am. Ceram. Soc., 57 (1974) 97.
[18] M. I. Osendi, J. S. Moya, C. J. Serna, J. SORIA, Metastability of tetragonal zirconia powders, J. Am. Ceram. Soc., 68 (1985) 135.
[19] B. Saad Al Farhan, Characterization of ZrO_2 Nano Particles Prepared by Glycothermal Method and their Efficiency as Adsorbent of As (III) and As (V) from Waste Water, J. Environ. Anal. Toxicol, 7 (2017) 532.
[20] G. Y. Guo, Y. L. Chen, Unusual structural phase transition in nanocrystalline zirconia, Appl. Phys. A, 84 (2006) 431.
[21] A. C. Bose, R. Ramamoorthy, S. Ramasamy, Formability of metastable tetragonal solid solution in nanocrystalline NiO-ZrO_2 powders, Mater. Lett., 44 (2000) 203.
[22] S. Gutzov, J. Ponahlo, C. L. Lengauer, A. Beran, Phase characterization of precipitated zirconia, J. Am. Ceram. Soc., 77 (1994) 1649.
[23] A. A. El-Fadl, M. Almokhtar, A. M. Nashaat, Synthesis, structural, optical, and magnetic properties of $ZnCr_{2-x}Fe_xO_4$ ($0\leq x\leq 0.8$) nanoparticles, Jpn. J. Appl. Phys., 57 (2018) 075001.
[24] A. A. El-Fadl, M. A. M. Hussien, A. S. Soltan, A. Abu-Sehly, Structure, optical and visible-light photocatalytic performance of $Mo_{1-x}Co_xS_2$ ($0\leq x\leq 0.1$) nanoparticles synthesized by facile hydrothermal method for methylene blue dye degradation, Dig. J. Nanomater. Bios., 19 (2024) 65.
[25] S. Chander, M. S. Dhaka, Impact of thermal annealing on physical properties of vacuum evaporated polycrystalline CdTe thin films for solar cell applications, Phys. E: Low-Dimens. Syst. Nanostructures., 80 (2016) 62.
[26] A. Abu El-Fadl, A. M. Eltokhey, A. A. Abu-Sehley, H. M. El-Attar, Fabrication and analysis of the structural phase transition of ZrO_2 nanoparticles using modified facile sol-gel route, Phase Trans., 92 (2019) 36.
[27] A. S. Keiteb, E. Saion, A. Zakaria, N. Soltani, Structural and optical properties of zirconia nanoparticles by thermal treatment synthesis, J. Nanomater., 2016 (2016) 1.
[28] W. Ahmed, J. Iqbal, S. O. Aisida, A. Badshah, I. Ahmad, K. Alamgir, I. H. Gul, Structural, magnetic and dielectric characteristics of optically tuned Fe doped ZrO_2 nanoparticles with visible light driven photocatalytic activity, Mater. Chem. Phys., 251 (2020) 1.
[29] V. Santos, M. Zeni, C. P. Bergmann, J. M. Hohemberger, Correlation between thermal treatment and tetragonal/monoclinic nanostructured zirconia powder obtained by sol-gel process, Rev. Adv. Mater. Sci, 17 (2008) 62.
[30] S. Nadeem, F. Iqbal, M. I. A. Mutalib, B. Abdullah, M. S. Shaharun, Synthesis and characterization of thermally stable zirconia based mesoporous nanosilica with metalloporphyrin encapsulation, AIP Conf. Proc., 1891 (2017) 1.
[31] K. Kaviyarasu, E. Manikandan, P. Paulraj, S. B. Mohamed, J. Kennedy, One

dimensional well aligned CdO nanocrystal by solvothermal method, J. Alloys Compd., 593 (2014) 67.
[32] J. Tauc, R. Grigorovici, A. Vancu, Optical properties and electronic structure of amorphous germanium, Phys. Status Solidi B, 15 (1966) 627.
[33] B. D. Viezbicke, S. Patel, B. E. Davis, D. P. Birnie III, Evaluation of the Tauc method for optical absorption edge determination: ZnO thin films as a model system, Phys. Status Solidi B, 252 (2015) 1700.
[34] G. Rajesh, S. Akilandeswari, D. Govindarajan, K. Thirumalai, Facile precipitation synthesis, structural, morphological, photoluminescence and photocatalytic properties of Ni doped ZrO_2 nanoparticles, Mater. Res. Express., 6 (2019) 1.
[35] S. Rani, S. Verma, S. Kumar, Tailoring the structural and optical parameters of zirconia nanoparticles via silver, Appl. Phys. A, 123 (2017) 1.